Direct Experimental Comparison of the Theories of Thermal and Optical Electron-Transfer: Studies of a Mixed-Valence Dinuclear Iron Polypyridyl Complex

C. Michael Elliott,* Daniel L. Derr, Dmitry V. Matyushov,† and Marshall D. Newton*

Contribution from the Department of Chemistry, Colorado State University, Ft. Collins, Colorado 80523, and Brookhaven National Laboratory, Upton, New York 11973

Received March 30, 1998

Abstract: The spectral parameters for the optically induced intervalence charge transfer and the rates of thermal electron transfer as a function of temperature have been measured for a rigid, triply linked mixed-valence dinuclear tris(2,2′-bipyridine)iron complex. The total reorganizational energy associated with the intramolecular electron exchange in this complex is almost exclusively outer-sphere in nature and comes from thermal fluctuations of the solvent. Thus, the system can be treated rigorously at the classical level, where in this context classical refers to treatments of the nuclear modes. The theories developed to describe the optical electron transfer and the thermal electron transfer are evaluated by analysis of the spectral and rate data, respectively. The quantities common to both theories are the donor−acceptor coupling matrix element, H_{12}, and the total reorganizational energy. Applying the respective theories to the appropriate corresponding sets of data yields reorganizational energies that are in excellent agreement irrespective of the manner in which the temperature dependence is treated; however, if the reorganizational energy is assumed to be temperature independent, H_{12}^{th} (from the rate data) and H_{12}^{op} (from the spectral data) differ by a statistically significant factor of ∼2.5. If the theoretically predicted temperature-dependent reorganizational energy composed of orientational reorganization of permanent dipoles and reorganization of solvent density is used in the calculations, the agreement between H_{12}^{op} and H_{12}^{th} improves dramatically. To our knowledge, this work constitutes the first attempt to experimentally compare these two classical theories with this level of rigor. Supplementing the experimental comparisons, we have conducted self-consistent-field (SCF) and configuration interaction (CI) calculations to obtain theoretical values of H_{12}^{op} and the donor−acceptor orbital separation, *r*, for comparison with experimentally determined values.

Introduction

Symmetric mixed-valence species, where the electron is localized on one site, undergo intramolecular electron self-exchange reactions which occur thermally or can be induced by absorption of light. The activation barrier for these processes arises from the free energies associated with the molecular (inner-sphere) and solvent (outer-sphere) reorganizations which occur upon electron transfer. Following the seminal work of Marcus, a variety of theoretical treatments have evolved relating the total reorganizational energy (λ) and the electronic coupling matrix element (H_{12}^{th}) to the rate of thermal electron exchange.[1,2] The assumptions made concerning the exchanging system and its external conditions determine the exact mathematical form of each theoretical expression. The semiclassical relationship, developed by Levich,[3] describes the rate of self-exchange in the case of a nonadiabatic system in the high temperature (classical) limit and is given by eq 1. This relation has the general form of an Arrhenius expression where the activation energy in the exponential term is equated to $\lambda/4$ as introduced by Marcus.[2]

$$k_{ET} = \frac{2(H_{12}^{th})^2}{h}\sqrt{\frac{\pi^3}{\lambda kT}}\, e^{-\lambda/4kT} \qquad (1)$$

In eq 1 k_{ET} is the rate constant for electron transfer, *h* is Planck's constant, *k* is the Boltzmann constant, and *T* is temperature.

The theory describing an optically induced electron transfer was developed by Hush.[4] In the two-state Mulliken formulation,[5] the donor−acceptor coupling matrix element (H_{12}^{op}) is related to the donor and acceptor orbital separation, *r*, and the following experimentally measurable quantities: the energy of the maximum, ν'_{IT}, the corresponding value of the extinction coefficient, ϵ'_{IT}, and the full width at half-maximum, $\Delta\nu'_{1/2}$ obtained from the intervalence transfer (IT) "reduced absorption spectrum"[4,6]

$$H_{12}^{op} = \frac{0.0206}{r}\sqrt{\epsilon'_{IT}(\Delta\nu'_{1/2})\nu'_{IT}(n^2/f(n))} \qquad (2)$$

where *r* is in Å, and H_{12}^{op}, and the spectral parameters are in

* Corresponding authors.
† Present address: University of Utah, Salt Lake City, UT 84112.

(1) Sutin, N. *Prog. Inorg. Chem.* **1983**, *30*, 441.
(2) Marcus, R. A. *J. Chem. Phys.* **1956**, *24*, 966.
(3) Levich, V. G. *Adv. Electrochem. Electrochem. Eng.* **1966**, *4*, 249.
(4) Hush, N. S. *Prog. Inorg. Chem.* **1967**, *8*, 391.
(5) (a) Mulliken, R. S. *J. Am. Chem. Soc.* **1950**, *72*, 600. (b) Mulliken, R. S. *J. Am. Chem. Soc.* **1952**, *74*, 811. (c) Mulliken, R. S. *J. Phys. Chem.* **1952**, *56*, 801.
(6) (a) Gould, I. R.; Noukakis, D.; Gomez-Jahn, L.; Young, R. H.; Goodman, J. L.; Farid, S. *Chem. Phys.* **1993**, *176*, 439. These authors present a more general vibronic model (their eq 4a) which is equiv to the present eq 2 in the high *T* limit. (b) Matyushov, D. V.; Ladanyi, B. M. *J. Phys. Chem. A* **1998**, *102*, 5027.

10.1021/ja981067d CCC: $15.00
Published on Web 10/28/1998

cm^{-1}. In eq 2 and throughout the remainder of this paper, the primed values indicate quantities associated with the reduced absorption spectrum (i.e., $\epsilon\nu$ vs ν), whereas nonprimed values refer to the unreduced spectrum (ϵ vs ν). Equation 2 also contains a refractive index correction, $(n^2/f(n))$. In the commonly used Birks and Chako formulations,[7] $f(n)$ is n^3 and $n(n^2 + 2)^2/9$, respectively, the Chako correction being the more rigorous theoretically.[7b,8]

While thermal and optical electron transfer generally pertain to different locations along the system reaction coordinate (respectively, the initial state equilibrium point and the transition state), H_{12}^{th} and H_{12}^{op} are usually assumed to be equal, in accord with the Condon approximation.[9] For a symmetric mixed-valence species, λ from eq 1 and ν'_{IT} from eq 2 can also be assumed to be equiv.[10] In principle, these two quantities, H_{12} and $\lambda \equiv \nu'_{IT}$, can be experimentally determined and compared by applying eqs 1 and 2 to appropriate rate and spectral data, respectively. In practice, making a direct experimental comparison of eqs 1 and 2 is not trivial. There are a few attempts at such a comparison in the literature,[11] although only the attempts of Nelsen and co-workers have been quantitative.[11b−f] In that work, however, the high-temperature limit in the thermal process (i.e., eq 1) was not applicable, and the inner sphere reorganization had to be treated nonclassically, complicating the interpretation of the results. Furthermore, the systems they studied do not approach the weak coupling limit, an assumption inherent in both eqs 1 and 2. Thus, a rigorous comparison of these two *classical* theories at the weak coupling limit has not previously been seriously attempted for the reasons outlined below.

First, eq 1 applies rigorously only to an electron self-exchange reaction; thus, the products and reactants are, by definition, identical. This fact, therefore, precludes employing any form of optical spectroscopy to follow the rate of electron exchange. One is consequently restricted in the means available for measuring the electron-transfer rate to techniques such as NMR line broadening (or related EPR experiments as in several of the previous reports cited above[11]). The ^{1}H NMR time scale places an upper limit of $\sim 1 \times 10^6$ s^{-1} on the rates accurately measurable with this technique,[12] which, in turn, necessitates that the donor and acceptor be fairly weakly coupled and/or that the electron transfer has a large reorganizational energy. The intensity of the optical transition, on the other hand, increases with the square of H_{12}^{op}, and the donor−acceptor coupling must be large enough for the IT transition to be detectable. These two requirements are at odds with one another, greatly limiting the number of mixed-valence systems that might yield both ascertainable rates of thermal electron transfer and measurable IT bands.

These purely experimental limitations aside, there are several additional considerations associated with the theoretical models underlying eqs 1 and 2 which also work against a rigorous comparison of the two theories. First, in comparing eqs 1 and 2 it must be assumed that the optical and thermal transitions occur between the same pair of nondegenerate potential energy surfaces. This is not always the case for symmetry or other reasons.[1] Second, it is not necessarily true that H_{12} is the same for the two types of processes. As noted above, in the thermal case the donor and acceptor wave functions, and thus H_{12}^{th}, are determined by the nuclear configuration in the transition state; for the optical case they are determined by the equilibrium nuclear coordinates. Especially in the case of inner-sphere coordinates, the larger the contribution to the total reorganizational energy, the greater one can expect the differences between H_{12}^{th} and H_{12}^{op} to be.[1] Spin−orbit coupling can also confuse the issue. Finally, there are often additional considerations which complicate, in particular, the interpretation of the optical data. These include, but are not limited to, specific solvent−solute interactions that are not accounted for by dielectric continuum theory[13] and uncertainty in the correct value of r appropriate for eq 2.[14−16] Given all of these caveats, it should not be surprising that only approximate comparisons between the theories engendering eqs 1 and 2 have so far been possible.

Herein we report studies on a unique dinuclear mixed-valence iron complex, **[Fe(440)$_3$Fe]$^{5+}$**. Partly by design and partly by

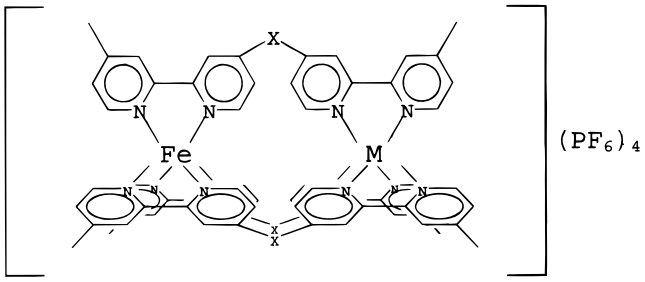

[Fe(440)$_3$Fe](PF$_6$)$_4$: M=Fe, X=(CH$_2$)$_4$
[Fe(440)$_3$Ru](PF$_6$)$_4$: M=Ru, X=(CH$_2$)$_4$
[Fe(430)$_3$Fe](PF$_6$)$_4$: M=Fe, X=(CH$_2$)$_3$
[Fe(420)$_3$Fe](PF$_6$)$_4$: M=Fe, X=(CH$_2$)$_2$

accident of nature, this specific complex constitutes a nearly ideal chemical system on which to base a rigorous comparison of the theories underlying eqs 1 and 2. First, it has proven possible with **[Fe(440)$_3$Fe]$^{5+}$** both to experimentally measure the rate of intermolecular electron exchange as a function of temperature and to observe and quantitate the IT band. Second, and of equal significance, the inner-sphere reorganizational energy associated with electron transfer in **[Fe(440)$_3$Fe]$^{5+}$** is, as we will argue subsequently, effectively zero. Thus, the system can be treated rigorously using a simple classical model and, as a consequence, many of the complications considered above (e.g., possible differences in H_{12}^{th} and H_{12}^{op}) simply vanish. As will become evident this dinuclear complex has

(7) (a) Birks, J. B. *Photophysics of Aromatic Molecules*; Wiley-Interscience: New York, 1970. (b) Hirayama, S.; Phillips, D. *J. Photochem.* **1980**, *12*, 139.

(8) (a) Gould, I. R.; Young, R. H.; Mueller, L. J.; Albrecht, A. C.; Farid, S. *J. Am. Chem. Soc.* **1994**, *116*, 3147. (b) Chako, N. Q. *J. Chem. Phys.* **1934**, *2*, 644. (c) Knoester, J.; Mukamel, S. *Phys. Rev. A* **1989**, *40*, 7065.

(9) (a) Newton, M. D. *Chem. Rev.* **1991**, *91*, 767. (b) Newton, M. D.; Cave, R. J. In *Molecular Electronics*; Jortner, J., Ratner, M. A., Eds.; Blackwell Science Ltd.: Oxford, 1997; p 73.

(10) Creutz, C.; Taube, H. *J. Am. Chem. Soc.* **1969**, *91*, 3988.

(11) (a) Ito, T.; Tomohiko, H.; Nagino, H.; Yamaguchi, T.; Washington, J.; Kubiak, C. P. *Science*, **1997**, *277*, 660. (b) Nelsen, S. F.; Adamus, J.; Wolff, J. J. *J. Am. Chem. Soc.* **1994**, *116*, 1589. (c) Nelsen, S. F.; Tamm, M. T.; Wolff, J. J.; Powell, D. R. *J. Am. Chem. Soc.* **1997**, *119*, 6863. (d) Nelsen, S. F.; Trieber, D. A., II; Wolff, J. J.; Powell, D. R.; Rogers-Crowly, S. *J. Am. Chem. Soc.* **1997**, *119*, 6873. (e) Nelsen, S. F.; Ismagilov, R. F.; Powell, D. R. *J. Am. Chem. Soc.* **1997**, *119*, 10213. (f) Nelsen, S. F.; Ismagilov, R. F.; Trieber, D. A., II *Science* **1997**, *278*, 846.

(12) Sandström, J. *Dynamic NMR Spectroscopy*; Academic Press: London, 1982.

(13) (a) Westmoreland, T. D.; Wilcox, D. E.; Baldwin, M. J.; Mims, W. B.; Soloman, E. I. *J. Am. Chem. Soc.* **1989**, *111*, 6106. (b) Brunschwig, B. S.; Ehrenson, S.; Sutin, N. *J. Phys. Chem.* **1986**, *90*, 3657. (c) Brunschwig, B. S.; Ehrenson, S.; Sutin, N. *J. Phys. Chem.* **1987**, *91*, 4714.

(14) (a) Oh, D. H.; Sano, M.; Boxer, S. G. *J. Am. Chem. Soc.* **1991**, *113*, 6880. (b) Hupp, J. T.; Dong, Y.; Blackbourn, R. L.; Lu, H. *J. Phys. Chem.* **1993**, *97*, 3278. (c) Karki, L.; Lu, H. P.; Hupp, J. T. *J. Phys. Chem.* **1996**, *100*, 15637.

(15) Karki, L.; Hupp, J. T. *J. Am. Chem. Soc.* **1997**, *119*, 4070.

(16) Cave, R. J.; Newton, M. D. *Chem. Phys. Lett.* **1996**, *249*, 15.

allowed us to conduct a comparison between these two theories with a level of rigor heretofore never attempted.

Finally, in addition to experimental considerations, **[Fe(440)$_3$Fe]$^{5+}$** has been treated theoretically at the self-consistent-field (SCF) and configuration interaction (CI) levels and analyzed using the generalized Mulliken−Hush (GMH) approach.[16] The results from this treatment confirm several of the experimental findings.

Experimental Section

Materials. Tetrakis(dimethyl sulfoxide)dichlororuthenium(II) (Ru(DMSO)$_4$Cl$_2$),[17] 1,4-bis-[4-(4′-methyl-2,2′-bipyridyl)]butane (**440**),[18] **[Fe(440)$_3$Fe](PF$_6$)$_4$**[18] and **[Fe(430)$_3$Fe](PF$_6$)$_4$**[18] were prepared as previously reported. All spectra were taken in acetonitrile-d_3 (ACN-d_3, Cambridge Isotope Laboratories, Andover, MA) solvent. All other materials were obtained from Aldrich Chem. Co., McCormick Distilling Co., or Fisher Scientific Co. and used as received, with the exception of nitrosonium tetrafluoroborate (Aldrich) which was vacuum-dried before use.

[Fe(440)$_3$Ru](PF$_6$)$_4$. Ru(DMSO)$_4$Cl$_2$ (57 mg, 120 μmol) in 20 mL of H_2O was added over 15 min to a 100-mL refluxing ethanol solution of **440** (936 mg, 2.37 mmol). An orange color developed immediately. After 2 h of stirring at reflux, the solvent was concentrated to 10 mL by rotary evaporation. The resulting slurry was treated with 50 mL of H_2O, and the excess ligand was removed from the orange solution by vacuum filtration. The reaction was repeated twice more with the recovered ligand using 28 mg (60 μmol) and 14 mg (30 μmol) Ru(DMSO)$_4$Cl$_2$ sequentially. The three water solutions were combined and heated to reflux. A solution of ferrous ammonium sulfate (84 mg, 210 μmol) in 20 mL of H_2O was added to the refluxing solution over half an hour. The resulting orange-red solution was stirred at reflux overnight. Heat was removed the reaction mixture filtered and the mother liquor treated with a few drops of saturated aqueous ammonium hexafluorophosphate. The solid crude product was isolated by vacuum filtration and purified using silica gel chromatography as previously reported[19] (4.1 mg, 1.0% by Ru). ^{1}H NMR (ACN-d_3, 25 °C): δ 8.40 (s, 3 H), 8.37 (s, 3 H), 8.34 (s, 3 H), 8.31 (s, 3 H), 7.53 (d, 6 H), 7.18 (m, 12 H), 6.99 (broad m, 6 H), 6.87 (d, 3 H), 2.91 (broad d, 6 H), 2.66 (broad t, 6 H), 2.53 (s, 9 H), 2.52 (s, 9 H), 1.80 (broad d, 6 H), 1.43 (broad q, 6 H). Visible spectrum (ACN-d_3, λ, nm (ϵ, M^{-1} cm^{-1})): 530 shoulder (9700), 464 (20000). MS (ES$^+$) *m*/*z*: 815.4 {**[Fe(440)$_3$Ru](PF$_6$)$_2^{2+}$**}, 495.3 {**[Fe(440)$_3$Ru](PF$_6$)$^{3+}$**}, 335.3 {**[Fe(440)$_3$Ru]$^{4+}$**}. Anal. Calcd for $C_{78}H_{78}N_{12}FeRuP_4F_{24}$: C, 48.78; H, 4.10; N, 8.75. Found: C, 49.04; H, 4.04; N, 8.80.

Nuclear Coordinate and Electronic Structure Calculations. All of the nuclear coordinates including the Fe−Fe distance in **[Fe(440)$_3$Fe]$^{4+}$** were determined from molecular dynamics and mechanics (MM) calculations as reported previously.[18] Electronic structure calculations were carried out using the all-valence electron INDO/S method[20] at the SCF and CI levels. The CI results were analyzed using the GMH approach,[16] as described in a previous study.[21]

Instrumentation. Nuclear magnetic resonance spectra were obtained on a Brüker AM-500 NMR spectrometer. Temperature for the NMR experiments was controlled with a BVT-1000 temperature control unit. Probe temperature was determined using a methanol NMR thermometer having an uncertainty of ±1 K (Wilmad Glass Company, Buena, NJ). Near-IR spectra were obtained on a Varian Cary 2400 spectrophotometer which was controlled by Spectra Calc (Galactic Industries, Salem, NH) on an interfaced computer. Temperature control for the spectral experiments was achieved using a Masterline 2095 cryostatic bath and circulator (Forma Scientific, Marietta, OH). In all of the low-temperature spectral experiments, a constant stream of dry Ar was flowed through the cell compartment. Near-IR spectra were manipulated and fit using Sigma Plot (Jandel Scientific, San Rafael, CA). NMR spectra were analyzed with Spectra Calc.

Spectrochemical Titration of [Fe(440)$_3$Fe]$^{n+}$. Under a nitrogen atmosphere, slightly more than 2 equiv of solid $NOBF_4$ was added to 5.0 mL of a 0.020 M solution of **[Fe(440)$_3$Fe](PF$_6$)$_4$**. The resulting green solution was gravity-filtered directly into a low volume 10-cm path length cell. An initial spectrum was recorded between 2200 and 800 nm. A small aliquot (∼0.2 equiv) of triethylamine (TEA) as a reducing agent was added to the cell, and the absorbance was monitored at 1000 nm. When the absorbance stabilized (after ∼1.5 h), a spectrum was recorded, and another aliquot of TEA was added to the cell. This procedure was repeated until no further spectral changes occurred between additions of reductant. A total of 13 spectra were acquired in this way during the titration. The temperature of the cell chamber of the spectrometer was 303 K.

Variable Temperature NMR of [Fe(440)$_3$Fe]$^{5+}$ and [Fe(440)$_3$Ru]$^{5+}$. Separate solutions of **[Fe(440)$_3$Fe](PF$_6$)$_4$** and **[Fe(440)$_3$Ru](PF$_6$)$_4$**, 1 mM, were prepared under a nitrogen atmosphere. Each solution was treated with less than 0.5 equiv of $NOBF_4$. Five NMR samples were then prepared from each of the original solutions: the initial concentration, and four dilutions, approximately 500 μM, 250 μM, 100 μM, and 50 μM. ^{1}H NMR of all 10 samples were taken at 230, 250, 270, 290, and 303 K.

Variable Temperature Spectral Studies of [Fe(430)$_3$Fe]$^{n+}$. A 0.02 M solution of **[Fe(430)$_3$Fe](PF$_6$)$_4$** was prepared under a nitrogen atmosphere. Spectra were taken (2950−650 nm) in a 1-cm path length cell at 270, 290, and 303 K. The solution was then oxidized with 2.0 equiv $NOBF_4$ under a nitrogen atmosphere, and spectra were taken at the same three temperatures. Subsequently, the solution was reduced with ∼1 equiv of TEA to generate the 5+ oxidation state, and spectra were again obtained over the same temperature range. Finally, the solution was completely reduced with an excess of TEA, and a room-temperature spectrum was recorded for comparison with that of the original solution.

Results

Structural Considerations. Despite a concerted effort, diffraction quality crystals of **[Fe(440)$_3$Fe]$^{4+}$** have not been obtained. It is necessary, then, to use techniques other than X-ray diffraction to determine this complex's structure. In the past, molecular dynamics and mechanics calculations have been shown to be useful in this regard for similar cations.[18,21,22]

Figure 1 is the lowest energy structure found when **[Fe(440)$_3$Fe]** is modeled with no anions present and the charge on every atom set at zero. The Fe−Fe distance, *d*, in this structure is 8.9 Å. As can be seen in Figure 1, all three bridges assume the same preferred orientation in this lowest energy structure. Of the 100 annealing runs carried out on this species, 6 produced a structure in the lowest energy well. Taking the mean and standard deviation of the Fe−Fe distance in these structures yields $d = 8.9 \pm 0.2$ Å. In the second-lowest energy well, one of the bridges becomes "kinked" while the other two remain in the preferred conformation, the energy increases by ∼6 kcal/mol (∼20kT), and *d* increases by 0.4 Å. Additional bridges becoming kinked further increases the total energy of the complex and *d*. **[Fe(440)$_3$Fe]** was also modeled in a number of other electrostatic environments: with a 4+ charge on the complex and various anions present (either constrained to specific positions or free to move) and with total zero charge

(17) Sullivan, B. P.; Salmon, D. J.; Meyer, T. J. *Inorg. Chem.* **1986**, *25*, 227.

(18) Ferrere, S.; Elliott, C. M. *Inorg. Chem.* **1995**, *34*, 5818.

(19) Elliott, C. M.; Freitag, R. A.; Blaney, D. D. *J. Am. Chem. Soc.* **1985**, *107*, 4647.

(20) (a) Zerner, M. C.; Loew, G. H.; Kirchner, R. F.; Mueller-Westerhoff, U. T. *J. Am. Chem. Soc.* **1980**, *102*, 589. (b) A comprehensive semiempirical SCF/CI package written by M. C. Zerner and co-workers, University of Florida, Gainesville, FL. (c) For an example of an application to thermal exchange between 2+/3+ transition metal ion complexes, see: Newton, M. D. *J. Phys. Chem.* **1991**, *95*, 30.

(21) Elliott, C. M.; Derr, D. L.; Ferrere, S.; Newton, M. D.; Liu, Y.-P. *J. Am. Chem. Soc.* **1996**, *118*, 5221.

(22) Larson, S. L.; Hendrickson, S. M.; Ferrere, S.; Derr, D. L.; Elliott, C. M. *J. Am. Chem. Soc.* **1995**, *117*, 5881.

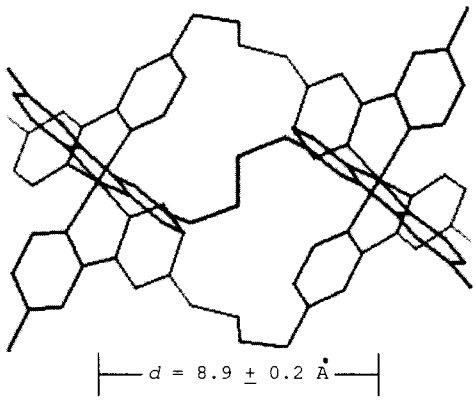

Figure 1. The measured Fe−Fe separation, *d*, and the lowest energy structure found from MM calculations on **[Fe(440)$_3$Fe]** with the charge on each atom set at zero. The lowest energy structure is independent of the electrostatic environment assumed in the modeling (see text), and thus, we believe this structure applies to the complex in all three oxidation states in solution.

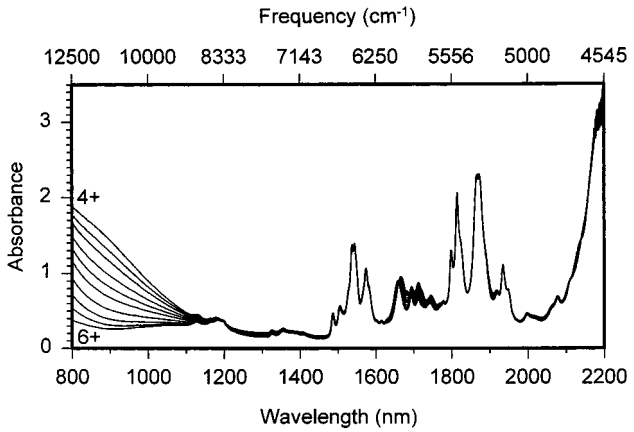

Figure 2. The near-IR spectral titration of **[Fe(440)$_3$Fe]$^{n+}$**. As the 6+ complex is reduced to 4+, the absorbance at high energy increases. The changes at wavelengths longer than 1100 nm are nearly indiscernible on this scale.

equilibrated over the complex and no anions present. Changing the electrostatic model does not in any way affect *d* or the bridge conformations in the lowest energy structure, nor does it affect the distance change upon a bridge becoming kinked. The only important parameter that is dependent on electrostatics is the difference in energy of the structures. The energy difference between the lowest and second-lowest energy structures becomes less when charges are included in the force field. From the fact that the electrostatic environment assumed in the modeling has no effect on the structural results, we assume that all three oxidation states, 4+, 5+, and 6+, have the same structure, shown in Figure 1.

Intervalence Charge-Transfer Transition of Mixed-Valence [Fe(440)$_3$Fe]$^{5+}$. Near-IR spectra taken at 303 K during the titration of **[Fe(440)$_3$Fe]$^{6+}$** with triethylamine are shown in Figure 2. The sharp peaks in the low energy region of the spectra are attributed to solvent and **[Fe(440)$_3$Fe]$^{n+}$** overtone vibrational bands, whereas the absorption at high energy which grows in during the titration is due to a relatively intense visible peak of **[Fe(440)$_3$Fe]$^{4+}$**. The weak absorbances due to the IT band in **[Fe(440)$_3$Fe]$^{5+}$** are obscured by these stronger absorptions. To obtain values for ν_{IT} and $\Delta\nu_{1/2}$, each spectrum was corrected to remove the solvent peaks and the transitions due to the individual trisdimethylbipyridineiron-like (FeL_3^{n+}) chromophores. After this correction, the remaining absorptions are due solely to an interaction between the FeL_3^{2+} and FeL_3^{3+} halves of the mixed-valence complex.

The general correction technique has been presented previously;[21] however, it has been somewhat altered in the present study. Initially, each raw spectrum taken during the titration had a weighted sum of the initial and final spectra subtracted from it. In other words, the initial spectrum (that of pure **[Fe(440)$_3$Fe]$^{6+}$**)[23] was multiplied by a coefficient, *C*, the final spectrum (that of pure **[Fe(440)$_3$Fe]$^{4+}$**)[23] was multiplied by $1 - C$, where $0 < C < 1$, and a weighted sum of this type was subtracted from each spectrum. An initial estimate of the coefficient *C* was made on the basis of the approximate progress of the titration. Its value was then varied until the best fit of the corrected spectrum was obtained to a model consisting of three Gaussian peaks. Three Gaussians were used in the model because the first correction attempts clearly indicated three distinct peaks in the region between 4550 and 12 500 cm^{-1}: (1) a band centered at ~5250 cm^{-1} with an approximate width of 70 cm^{-1} (vide infra), (2) the low energy tail of a visible band located at ~15 500 cm^{-1} with an approximate width of 3500 cm^{-1} (vide infra), and (3) the IT band itself. The various peak parameters obtained from this initial fit were entirely reasonable. However, upon careful examination there were small systematic variations over the course of the titration in the position and width of both the visible absorption and the IT band. Since there appears to be no chemically reasonable explanation for this, it was assumed to be an artifact of the fit.

Consequently, the fitting approach was slightly modified. It is clear from the initial fit that only the 15 500 cm^{-1} band contributes significantly to the absorbance in the region between 12 000 and 12 500 cm^{-1} (the high energy end of the spectra in Figure 2). Therefore, this spectral region was refit to the tail of a single Gaussian peak, and *C* was again varied until the best fit was obtained. Reassuringly, the values of *C* for each spectrum did not change significantly from the values obtained in the initial fits of the whole spectra. Moreover, there was no evidence of any systematic variation in either the energy or width of the visible peak. The average peak position and width thus obtained were 15 400 ± 200 cm^{-1} and 3500 ± 200 cm^{-1}, respectively. A similar process was used to determine the position and width of the peak at 5250 cm^{-1}, yielding an energy of 5253 ± 1 cm^{-1}, and a width of 73 ± 3 cm^{-1}.

Fits of the whole spectral range to three Gaussians were then carried out again but with the position and width of both the visible and overtone vibrational peaks fixed at the above values. To correct for a slight negative baseline in some of the corrected spectra taken early in the titration, the average absorbance in the region 4875−4955 cm^{-1} (a flat portion of the spectra with good signal-to-noise characteristics) was set to zero prior to each of these later fits. The heights of all three peaks, and ν_{IT} and $\Delta\nu_{1/2}$ were allowed to vary. Again, *C* changed very little with the alteration of the fit, and the systematic variation in $\Delta\nu_{1/2}$

(23) The titration endpoints are not necessarily the first and last spectra taken. A small excess of $NOBF_4$ was used to initially oxidize **[Fe(440)$_3$Fe]$^{4+}$** to **[Fe(440)$_3$Fe]$^{6+}$**. Thus, early in the titration, any spectral changes seen appear to not correspond to changes in the oxidation state of **[Fe(440)$_3$Fe]$^{n+}$**. Additionally, since the amount of reductant in each aliquot was not quantitatively determined, the endpoint cannot be predicted, a priori. A few extra spectra at the end of the titration were taken to ensure that reduction was truly complete. These extra spectra, both at the beginning and at the end of the titration, were discarded. The actual endpoints were determined by using the correction procedure outlined in the text. The spectrum obtained before the first spectrum in the titration to exhibit an IT band (after correction) was taken as the initial spectrum. Similarly, the spectrum obtained after the last spectrum with a detectable IT band was taken to be the final endpoint. The intervening spectra were then corrected as described in the text using these initial and endpoint spectra.

Table 1. Peak Parameters for the IT Band Found in the Titration of $[Fe(440)_3Fe]^{6+}$ by Triethylamine

spectrum	ν_{IT} (cm^{-1})[a]	$\Delta\nu_{1/2}$ (cm^{-1})[a]	corrected absorbance ($\times 10^2$)[a]
2	7490 ± 50	3300 ± 100	1.12 ± 0.03
3	7600 ± 30	3550 ± 60	1.94 ± 0.03
4	7500 ± 20	3360 ± 40	2.55 ± 0.03
5	7410 ± 20	3280 ± 40	2.79 ± 0.03
6	7420 ± 20	3070 ± 40	2.75 ± 0.03
7	7450 ± 20	2940 ± 60	2.50 ± 0.04
8	7380 ± 30	2950 ± 80	1.84 ± 0.03
9	7480 ± 40	3000 ± 100	1.15 ± 0.03
average	7470 ± 60	3200 ± 200	

[a] All values were obtained from the fits of the corrected spectra, as described in the text.

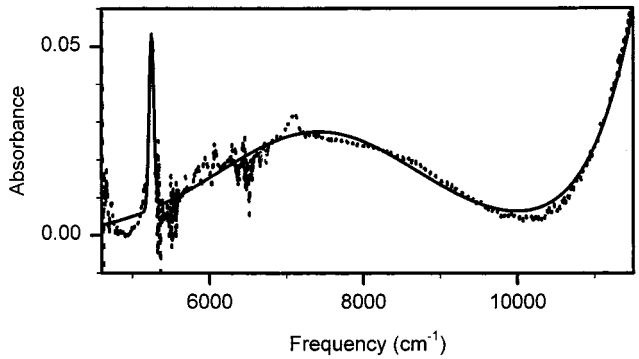

Figure 3. One of the spectra taken near the middle of the titration (Spectrum 6) of $[Fe(440)_3Fe]^{n+}$, corrected as described in the text. The dotted line is the experimental data, and the solid line is the best fit of these data to three Gaussians. The broad band centered at ~7500 cm^{-1} is the IT band.

was now absent. The parameters describing the Gaussian corresponding to the IT band for each corrected spectrum are summarized in Table 1.

To test the sensitivity of the IT peak parameters to the shape of the visible peak, its position and width were varied by $\pm\sigma$ and spectrum 6 was refit. The values thus obtained for ν_{IT} and $\Delta\nu_{1/2}$ were still within one standard deviation of the original results, indicating only a weak interdependence of these two peaks in the fit. Averaging the values in Table 1 gives $\nu_{IT} = 7470 \pm 60$ cm^{-1} and $\Delta\nu_{1/2} = 3200 \pm 200$ cm^{-1}. It is comforting to note that the average values of ν_{IT} and $\Delta\nu_{1/2}$ resulting from the final fits are quite similar to those obtained from the initial fitting attempt but without any systematic variation evident over the course of the titration. Spectrum 6, corrected and truncated to illustrate the IT band, is shown in Figure 3 along with the fit.

Figure 4 is a plot of absorbance at ν_{IT} (1330 nm, determined from the fits described above) vs the absorbance at 800 nm, both taken from the raw spectra (Figure 2). Plots of this type are used to obtain the extinction coefficient for the IT band, ϵ_{IT}.[21] The shape of the curve in Figure 4 is determined by 7 parameters: the extinction coefficients of all three oxidation states of the complex at both wavelengths ($\epsilon_{n+,\lambda}$), and the comproportionation constant, K_{com}, for eq 3. Two of the

$$[Fe(440)_3Fe]^{4+} + [Fe(440)_3Fe]^{6+} \rightleftharpoons 2[Fe(440)_3Fe]^{5+} \quad (3)$$

extinction coefficients, $\epsilon_{4+,800}$ and $\epsilon_{6+,800}$, were taken directly from the end points of the titration, and K_{com} was determined electrochemically.[18] The remaining four extinction coefficients, $\epsilon_{4+,1330}$, $\epsilon_{6+,1330}$, $\epsilon_{5+,800}$, and $\epsilon_{5+,1330}$, were determined from the best fit of the experimental data in Figure 4 to an expression

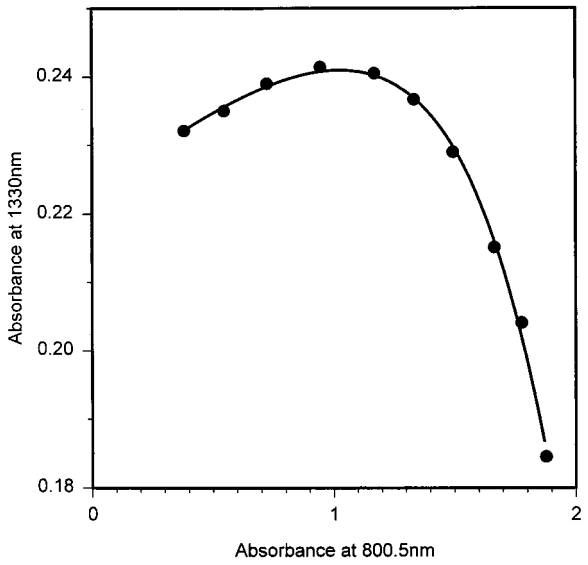

Figure 4. Plot of absorbance data used to determine ϵ_{IT}. The solid circles are the experimental data, and the curve is the best fit using an expression developed from Beer's Law, mass balance, and the equilibrium expression.[21]

derived from Beer's Law, mass balance, and the comproportionation equilibrium expression.[21,24] The extinction coefficient of the IT band, ϵ_{IT}, is then obtained by correcting $\epsilon_{5+,1330}$ for the residual absorbance from the individual FeL_3^{2+} and FeL_3^{3+} chromophores using eq 4

$$\epsilon_{IT} = \epsilon_{5+,1330} - \frac{\epsilon_{4+,1330} + \epsilon_{6+,1330}}{2} \quad (4)$$

The value of ϵ_{IT} resulting from the fit of the experimental data in Figure 4 (the solid line) is 0.24 ± 0.01 M^{-1} cm^{-1}. Fits using different monitoring wavelengths (i.e., the *x* axis in Figure 4) are all in perfect agreement. Furthermore, altering the fit equation to use the intensities in Table 1 also produces the same value of ϵ_{IT}. Since the different fitting procedures each give the same result, we are fully confident that the value of ϵ_{IT} is 0.24 ± 0.01 M^{-1} cm^{-1}, despite its small magnitude.

Thermal Electron Transfer in $[Fe(440)_3Fe]^{5+}$. The intramolecular electron-transfer process in $[Fe(440)_3Fe]^{5+}$ exchanges the magnetic environment in the two halves of the molecule, so that the rate constant of the exchange mechanism, in this case k_{ET}, can, in principle, be determined from ^1H NMR line shape analysis.[25] Similar measurements have been made to obtain bimolecular self-exchange rate constants for $Fe(DMB)_3^{3+/2+}$ (where DMB is 4,4′-dimethyl-2,2′-bipyridine).[26] For $[Fe(440)_3Fe]^{5+}$, over the temperature range studied, the intramolecular electron-transfer rate is near the fast exchange limit of the NMR time scale; thus, a single broadened peak results for each pair of exchanging nuclei. To determine the rate of this exchange, the peak positions and line widths in the absence of exchange need to be determined. Often these parameters can be obtained by lowering the temperature and

(24) Two more extinction coefficients, $\epsilon_{6+,1330}$ and $\epsilon_{4+,1330}$, could also have been obtained from the initial and final titration spectra, respectively. However, given the signal-to-noise ratio of these spectra and the fact that the fit is significantly over-determined, these parameters were obtained from the fit.

(25) (a) Gutowsky, H. S.; Saika, H. *J. Chem. Phys.* **1953**, *21*, 1688. (b) Gutowsky, H. S.; Holm, C. H. *J. Chem. Phys.* **1956**, *25*, 1288. (c) Reeves, L. W. *Adv. Phys. Org. Chem.* **1965**, *3*, 187. (d) Johnson, C. S. *Adv. Magn. Reson.* **1965**, *1*, 33.

(26) Chan, M.-S.; Wahl, A. C. *J. Phys. Chem.* **1978**, *82*, 2542.

shutting down the exchange process. However, in the present case, this is not possible. At 230 K, just 5 K above the melting point of the acetonitrile solvent, all of the peaks are still coalesced. Consequently, a different approach is required.

For the very closely related complex $\mathbf{[Fe(440)_3Ru]}^{n+}$, the difference in potential for the $Ru^{3+/2+}$ and $Fe^{3+/2+}$ couples, $\Delta E_{1/2}$, is ~200 mV[27] while $\Delta E_{1/2}$ for the corresponding $\mathbf{[Fe(440)_3Fe]}^{6+/5+}$ and $\mathbf{[Fe(440)_3Fe]}^{5+/4+}$ couples is only about 52 mV.[18] In the latter case, the separation of the electrochemical waves is purely due to the electrostatic interaction of the two otherwise identical iron centers,[18] but in the former, the difference in $E_{1/2}$'s results primarily from the electron affinity difference between ruthenium and iron. As a consequence of this relatively large $\Delta E_{1/2}$, no significant intramolecular electron exchange occurs between the Ru^{2+} and Fe^{3+} metal centers. Even at room temperature, the electron remains localized on the ruthenium metal center.

As anticipated, NMR spectra of $\mathbf{[Fe(440)_3Ru]}^{5+}$ exhibit ^{1}H resonances corresponding to the separate halves of the molecule; peaks resulting from the diamagnetic Ru(II) side of the molecule have widths and chemical shifts that are nearly identical to those of $[Fe(DMB)_3]^{2+}$, and resonances arising from the Fe(III) half of the molecule are significantly paramagnetically shifted and broadened, as they are in the spectrum of $[Fe(DMB)_3]^{3+}$. In the calculations described below, the chemical shift and peak widths of $\mathbf{[Fe(440)_3Fe]}^{5+}$ in the absence of electron exchange were assumed to be the same as those measured for $\mathbf{[Fe(440)_3Ru]}^{5+}$.

If the electron-transfer process is assumed to be near the fast exchange limit on the NMR time scale and a simple equal-population, two-site model is used, the rate constant for exchange can be calculated from eq 5, which is a modified version of eq 2.24 in ref 12,

$$k_{ET} = \frac{\pi(\nu_{Fe(III)} - \nu_{Ru(II)})^2}{2\Delta\nu_{1/2,Fe(III,II)} - \Delta\nu_{1/2,Fe(III)} - \Delta\nu_{1/2,Ru(II)}} \qquad (5)$$

where ν's correspond to peak positions and $\Delta\nu_{1/2}$'s peak widths at half-maximum, both in Hz. The only resonances available in the proton spectrum for such an analysis are those from the methyl group and from a bridging methylene proton. The remaining peaks from the bridge protons are buried under other resonances in one oxidation state or another, and the aromatic resonances either do not shift enough to show significant exchange broadening in the mixed-valence spectrum or are so broad that they are undetectable at the low concentrations necessary to ensure an absence of intermolecular electron exchange. The methyl and methylene peaks in all three oxidation states at 270 K for the 500 μM samples are displayed in Figure 5.

The methyl peaks are, of course, singlets and straightforwardly yield the parameters in eq 5 by fitting them to a Lorentzian line shape. The methylene peak, on the other hand, is at best a triplet, considerably complicating the determination of the widths of the paramagnetically and exchange-broadened peaks. Since the broadening is greater than the splitting in these signals, only a single structureless peak results, and it is impossible to know what the J coupling is. Inspection of the Ru(II) methylene resonance for $\mathbf{[Fe(440)_3Ru]}^{5+}$ in all of the spectra used in the rate calculations produces a splitting of ~7.5 Hz, whereas the corresponding splitting in $\mathbf{[Fe(440)_3Fe]}^{4+}$ is ~10 Hz. It is unclear which, if either of these values would be appropriate to use in fitting the paramagnetically and exchange-broadened peaks. At the lowest two temperatures studied, the broadening due to paramagnetic and exchange effects is large enough that the uncertainty in the J coupling is insignificant. The rates calculated from the methylene peak are within experimental error of those obtained from the methyl peak at these temperatures. However, at higher temperatures the broadening is on the same order of magnitude as the uncertainty in J, and there is poor agreement between the rates calculated from the two different resonances if a J of 7.5 Hz is assumed. Since J is not known for this triplet peak and the model used to determine electron transfer rates from the methyl resonance is much less ambiguous, only these rates (collected in Table 2) are considered below in the application of eq 1.

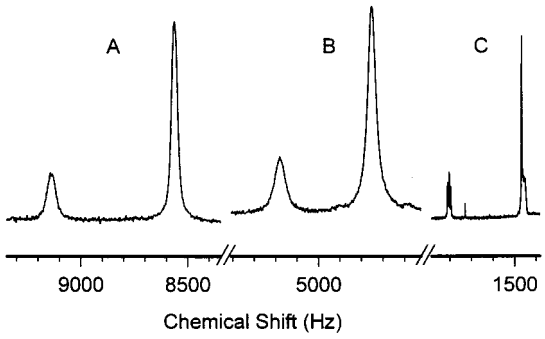

Figure 5. The methyl and a methylene ^{1}H NMR peak from the 500 μM samples at 270 K. Spectrum B is from a solution of $\mathbf{[Fe(440)_3Fe]}^{5+}$. Spectra A and C are from a single solution of $\mathbf{[Fe(440)_3Ru]}^{5+}$. Spectrum C shows the protons on the diamagnetic Ru^{2+} half and spectrum A, the paramagnetic Fe^{3+} half. Spectrum B shows the coalesced resonances from both halves of $\mathbf{[Fe(440)_3Fe]}^{5+}$. In panel C, the broad base on the upfield side of the methyl peak is the resonance associated with one of the protons in the bridge of $\mathbf{[Fe(440)_3Ru]}^{4+}$, which is also present in solution.

Table 2. Rate Constants for Electron Self-Exchange in $\mathbf{[Fe(440)_3Fe]}^{5+}$ Determined from ^{1}H NMR Line Shape Analysis

temperature (K)	k_{ET} (s^{-1})[a]
230	$4.9 \pm 0.2 \times 10^5$
250	$1.24 \pm 0.02 \times 10^6$
270	$3.1 \pm 0.2 \times 10^6$
290	$5.1 \pm 0.3 \times 10^6$
303	$7.1 \pm 0.6 \times 10^6$

[a] Rate constants were calculated from eq 5 using peak parameters from the fit of the methyl resonance to a single Lorentzian line shape.

Dependence of the Intervalence Transfer Band of $\mathbf{[Fe(430)_3Fe]}^{5+}$ on Temperature. While it has often been assumed that λ has negligible temperature dependence, recent experimental studies have indicated that it may in fact vary appreciably with temperature,[28] although, in other cases the temperature dependence appears to be quite small.[29] It is an important theoretical challenge to be able to predict the sign as well as the magnitude of the temperature derivative, $(\partial\lambda/\partial T)_P$, where the subscript P refers to the isobaric conditions appropriate to the experiment. For reasonably polar solvents, continuum theories (e.g., the 2-sphere Born-type model of Marcus,[30a] or the 1-sphere reaction field model of Onsager[30b]) tend to predict

(27) Ferrere, S., Ph.D. Thesis, Colorado State University, 1994.

(28) (a) Liang, N.; Miller, J. R.; Closs, G. L. *J. Am. Chem. Soc.* **1989**, *111*, 8740. (b) Kumar, K.; Kurnikov, I. V.; Beratan, D. N.; Waldeck, D. H.; Zimmt, M. B. *J. Phys. Chem.* **1998**, *102*, 5529. (c) Vath, P.; Zimmt, M. B.; Matyushov, D. V., to be submitted. (d) Vath, P.; Zimmt, M. B., in preparation.

(29) Dong, Y.; Hupp, J. T. *Inorg. Chem.* **1992**, *31*, 3322.

(30) (a) Marcus, R. A. *J. Chem. Phys.* **1965**, *43*, 679. (b) Onsager, L. *J. Am. Chem. Soc.* **1936**, *58*, 1486. (c) *Handbook of Chemistry and Physics*, 56th edition; Weast, R. C., Ed.: CRC Press: Cleveland, 1976.

positive $(\partial\lambda/\partial T)_P$ values. On the other hand, experimental results for both weakly and moderately polar solvents yield several examples of negative $(\partial\lambda/\partial T)_P$.[28]

In an attempt to determine how λ varies with temperature for **[Fe(440)$_3$Fe]$^{5+}$**, the temperature dependence of the IT band in the closely related mixed-valence complex, **[Fe(430)$_3$Fe]$^{5+}$**, was examined. This complex was chosen for study because of its close structural similarity to **[Fe(440)$_3$Fe]$^{5+}$** and the fact that the extinction coefficient for its IT transition is ~2 orders of magnitude larger. Despite this larger extinction coefficient, certain ambiguities in the data prevent us from quantifying the value of $(\partial\lambda/\partial T)_P$; nonetheless, careful examination of the corrected (vide supra) IT spectra of **[Fe(430)$_3$Fe]$^{5+}$** indicates a shift toward higher energy as the temperature is lowered from 303 to 270 K, suggesting a negative value for $(\partial\lambda/\partial T)_P$. Presently, efforts are under way to quantify $(\partial\lambda/\partial T)_P$ for this and other related mixed-valence dimers.

Discussion

The objective of this study is, again, to compare the electronic coupling matrix element, H_{12}, and reorganizational energy obtained independently from measurements of the optical intervalence electron transfer and the rate of thermal electron exchange in **[Fe(440)$_3$Fe]$^{5+}$**. As we stated in the Introduction, attempts to make this type of direct comparison previously have been hampered by complications inherent in the chemical systems studied. In contrast, the **[Fe(440)$_3$Fe]$^{5+}$** complex is free of many such complications and is a nearly ideal chemical vehicle for making this comparison. However, it is important to understand the limitations that do remain with this system.

There are several assumptions common to eqs 1 and 2 that require some critical evaluation. The most obvious question concerns whether the classical harmonic model is appropriate. A purely classical treatment is not possible if the inner sphere reorganization involves moderate to high frequency vibrational modes that must be treated quantum mechanically. In the present case this is a moot point, since there is essentially no inner-sphere contribution to the reorganizational energy. There are no structural differences between $[Fe(bpy)_3]^{2+}$ and $[Fe(bpy)_3]^{3+}$ (where bpy is 2,2′-bipyridine), based on a comparison of crystallographic data for the two oxidation states of the complex. The same can be said for $[Fe(phen)_3]$ (where phen is 1,10-phenanthroline).[31] Consistent with the crystallographic data, vibrational spectra of these ions also show very little change in the Fe−N stretching frequencies upon oxidation from 2+ to 3+.[32] Apparently, the decrease in metal-to-ligand π back-bonding is exactly counterbalanced by the increase in σ donation upon oxidation from the 2+ to the 3+ oxidation state. Since the local environments of the two individual metal centers in **[Fe(440)$_3$Fe]$^{5+}$** are virtually identical to those of $[Fe(bpy)_3]^{2+}$ and $[Fe(bpy)_3]^{3+}$, it is reasonable to conclude that any inner-sphere reorganization in **[Fe(440)$_3$Fe]$^{5+}$** is negligible. The outer-sphere component then, made up of thermal solvent fluctuations, dominates the reorganizational energy. In the absence of dielectric saturation, the classical harmonic models utilized in this study should be entirely valid. In the present case, dielectric saturation is hardly conceivable since the complex radius is ~4.5 Å, the effective solvent radius is ~2 Å, and the charge-dipole separation is ≥6.5 Å.

In **[Fe(440)$_3$Fe]$^{5+}$**, the ligand field about each metal has approximate C_3 symmetry. This trigonal distortion of O_h symmetry splits the t_{2g} hole states into a spatially nondegenerate A and a doubly degenerate E state.[33] We denote this splitting by Δ (defined as positive when the A state lies below the E state).[33] While the Δ value for the $Fe(bpy)_3^{3+}$ moiety in the **[Fe(440)$_3$Fe]$^{5+}$**complex is not known, the value of 120 cm^{-1} obtained for the isolated $[Fe(bpy)_3]^{3+}$ complex[35] may be taken as a plausible estimate, since the local coordination of the Fe^{3+} sites is very similar in the two complexes. In the A state the hole is localized in the d_z^2-type atomic orbital (AO) of the Fe^{3+} site, where z corresponds to the Fe−Fe vector (the quasi 3-fold axis). Spin−orbit coupling also splits the t_{2g} hole state degeneracy. The value of the spin−orbit coupling constant, λ_{SO}, obtained from low-temperature EPR spectra, has been reported to be ~440 cm^{-1} for $[Fe(bpy)_3]^{3+}$.[33,34] This value is small, relative to values of λ_{SO} for the second- and third-row metals, but must be taken into account together with Δ in formulating the relevant states involved in the electron-transfer processes under consideration here. Using the above values of Δ and λ_{SO} and the analysis of ref 33 we find that spin−orbit coupling mixes the A state with one component of the E state (denoted E′), yielding a ground state (Ψ_1), comprised of 58% E′ and 42% A, and an excited state (Ψ_2), with 58% A and 42% E′ character) lying 630 cm^{-1} (or 3.0kT) above the ground state. The other E component (Ψ_3 denoted E″) is unmixed and lies 700 cm^{-1} (3.4kT) above Ψ_1. Thus, at room temperature, thermal occupation of the higher states Ψ_2, Ψ_3 may be neglected (<5%) in the analysis given below. We also note that Ψ_1, Ψ_2, and Ψ_3 are each doubly degenerate.

Optical Electron Transfer. The spectral line shape can be understood in terms of the charge-localized states introduced above (Ψ_1, Ψ_2, and Ψ_3). In the limiting case where the two coordination complexes are "eclipsed" (i.e., with vanishing N−Fe−Fe′−N′ torsional angles, ϕ, where N and N′ refer to the nitrogen atoms in the respective inner pyridines of a given bridging ligand), a common Cartesian coordinate system (e.g., the one adopted in ref 33) may be employed for the charge-localized states at each Fe site, and the overall line shape is a superposition of two slightly displaced transitions, i.e., those connecting the charge-localized ground state Ψ_1 at one coordination site with, respectively, the corresponding ground state Ψ_1 and the first excited state, Ψ_2, at the other site. The intensity of the perpendicularly polarized IT process connecting Ψ_1 and Ψ_3 is found negligible (on the basis of INDO/S calculations[20]) in comparison with that for the other two transitions. The peak separation of the two transitions is the $\Psi_1-\Psi_2$ splitting (i.e., 630 cm^{-1} as given above). Since this splitting is relatively small, it is convenient in the following analysis to treat the broad observed IT spectral line shape effectively as a single transition with an effective transition moment given by the following root-mean-square (rms) expression:

$$\mu_{\text{eff}} \equiv \sqrt{(\cos\theta)^2(\mu_A)^2 + (\sin\theta)^2(\mu_{E'})^2} \qquad (6)$$

where $\cos\theta = (0.58)^{1/2}$ is the spin−orbit mixing coefficient (see above) and where μ_A ($\mu_{E'}$) is the transition moment connecting the charge-localized A (E′) states at the two Fe sites. In fact, INDO/S calculations[20] of the type described below indicate that μ_A and $\mu_{E'}$ have similar magnitudes ($|\mu_A| \cong 0.9|\mu_{E'}|$). In terms of the transition moments for the $\Psi_1 \rightarrow \Psi_1$

(31) (a) Healy, P. C.; Skelton, B. W.; White, A. H. *Aust. J. Chem.* **1983**, *36*, 2057. (b) Figgis, B. N.; Skelton, B. W.; White, A. H. *Aust. J. Chem.* **1978**, *31*, 57. (c) Zalkin, A.; Templeton, D. H.; Ueki, T. *Inorg. Chem.* **1973**, *12*, 1641. (d) Baker, J.; Engelhardt, L. M.; Figgis, B. N.; White, A. H. *Chem. Soc., Dalton Trans.* **1975**, 530.

(32) Saito, Y.; Takemoto, J.; Hutchinson, B.; Nakamoto, K. *Inorg. Chem.* **1972**, *11*, 2003.

(33) Kober, E. M.; Meyer, T. J. *Inorg. Chem.* **1983**, *21*, 3967.

(34) In local octahedral symmetry, λ_{SO} corresponds to a state splitting of $^3/_2\lambda_{SO} = 660$ cm^{-1}.

(35) Kober, E. M.; Meyer, T. J. *Inorg. Chem.* **1982**, *22*, 1614.

($\mu_{1\rightarrow1}$) and $\Psi_1 \rightarrow \Psi_2$ ($\mu_{1\rightarrow2}$) IT transitions, μ_{eff} is equivalent to $(\mu_{1\rightarrow1}^2 + \mu_{1\rightarrow2}^2)^{1/2}$.

Analogous to the above situation for transition moments, the effective coupling element, H_{12}^{op}, may be viewed as a rms quantity based on the coupling elements for the A $\rightarrow$ A and E′ $\rightarrow$ E′ processes (for the cases considered here, a given coupling element H_{12}^{op} is essentially proportional[4−6] to the corresponding transition movement (μ_{eff}, μ_{A}, or $\mu_{\text{E}'}$).

If the torsional angles ϕ relating the two coordination spheres depart from zero (as discussed below), the above treatment leading to eq 6 must be generalized. Nevertheless, even with such refinements it should still be reasonable to treat the overall (superposition) line shape as that of a single effective transition, whose maximum corresponds to a weighted sum of the contributions from the two primary transitions (ground to ground and ground to first excited state). The consequences of these assumptions for the analysis based on eq 2 will be quite minor, since the experimental band will retain nearly the same position, shape, and integrated area as it would have were it composed of a pure single transition.

The spectral parameters obtained from the band after converting it to a reduced absorption spectrum are the values needed in the application of eq 2.[6,36] Taking the average of the values in Table 1 yields $\nu_{\text{IT}} = 7470 \pm 60$ cm^{-1}. For a symmetric complex, $\Delta\nu_{1/2}$ should be related to the position of the IT band maximum at 303 K by eq 7

$$\Delta\nu_{1/2} = \sqrt{2335(\nu_{\text{IT}})} \qquad (7)$$

where $\Delta\nu_{1/2}$ and ν_{IT} are in cm^{-1}.[4,37]

Application of this relation gives $\Delta\nu_{1/2} = 4180 \pm 20$ cm^{-1}. The value of $\Delta\nu_{1/2}$ resulting from the average of the data in Table 1 is 3200 ± 200 cm^{-1}. The origin of this discrepancy is not immediately clear, although differences between theoretical (from eq 7) and experimental values of $\Delta\nu_{1/2}$ are not uncommon. They often arise from system nonidealities with respect to the model (e.g., large spin−orbit contributions to ν_{IT} for second and third row transition metals, or anharmonicity), but they almost always result in the experimental value being too large.[38] The near ideality of the **[Fe(440)$_3$Fe]**$^{5+}$ system and the fact that the calculated value of $\Delta\nu_{1/2}$ is larger than the experimental value suggests other origins for the discrepancy in the present case, most likely arising from an artifact of the spectral fitting. There was significant spectral manipulation necessary to obtain the bandwidths collected in Table 1. Specifically, in the final fit, a constant absorbance was added to each spectrum to correct for what appeared to be a nonzero baseline (i.e., an offset of the absorbance). The absorbance from 4875 to 4955 cm^{-1} was adjusted to an average value of zero, and this region was chosen because it has good signal-to-noise characteristics, and is fairly flat. Inspection of Figure 3 reveals, however, that this region probably contains a small contribution from the tail of the fitted IT band. Setting the absorbance at zero in this region, then, is not entirely correct. It was deemed that further attempts to improve this background correction would only serve to complicate the already nontrivial interpretation of the fit results. It should be emphasized, however, that, the only peak parameter used in eq 2 that is sensitive to the baseline correction is $\Delta\nu_{1/2}$; ν_{IT} did not change upon addition of this baseline correction to the model used in the fit, and ϵ_{IT} was determined from a completely different treatment. Thus, the value of $\Delta\nu_{1/2} = 4180 \pm 30$ cm^{-1} obtained from eq 7 is probably the more reliable value to use in obtaining the reduced absorption spectrum. In any case, while the experimental and predicted values for $\Delta\nu_{1/2}$ are not within the calculated statistical errors of each other, the difference is only ∼20%, which, in the final analysis, has little effect on the calculated value of H_{12}^{op} (vide infra) using eq 2.

The accuracy of ϵ_{IT} was discussed in detail in the Results section. Analysis of the full spectral fits was used to determine ν_{IT}, and it is clear from the fit results that only the IT band has significant absorbance at ν_{IT}; however, it should be reiterated here that ϵ_{IT} *is not* obtained from the same fit as the other IT peak parameters. Thus, any problems that might be associated with the three Gaussian model do not impact on the determination of ϵ_{IT}.

Finally, some comment about the likely origin of the extra peaks in this three Gaussian model (i.e., the visible absorption at 15400 cm^{-1} and the peak at 5250 cm^{-1}) is in order. The visible band shows up near the red edge of the MLCT transition of the FeL_3^{2+} chromophore. In the fully reduced complex, each FeL_3^{2+} chromophore has as its nearest neighbor another FeL_3^{2+} moiety, whereas in the mixed-valence complex, the nearest neighbor is an FeL_3^{3+} site. It is quite likely that the difference between the electrostatic environments of the FeL_3^{2+} chromophores in **[Fe(440)$_3$Fe]**$^{4+}$ and **[Fe(440)$_3$Fe]**$^{5+}$ would produce slight changes in the energies or intensities of the MLCT and $d-d$ bands which would be expected to yield a peak in the spectra corrected in the manner described above.

The appearance of the overtone vibration at 5250 cm^{-1} can be rationalized similarly on the basis of symmetry arguments. The lack of a differential peak shape for the 5250 cm^{-1} peak argues that this transition is the result of an increase in oscillator strength for a vibration rather than a shift in energy. This increase in oscillator strength could reasonably arise from the reduced electrostatic symmetry of **[Fe(440)$_3$Fe]**$^{5+}$ compared to that of **[Fe(440)$_3$Fe]**$^{4+}$ and **[Fe(440)$_3$Fe]**$^{6+}$, where the two metal centers are symmetry related. On the vibrational time scale, in **[Fe(440)$_3$Fe]**$^{5+}$, the two halves of the molecule are no longer equiv because of the charge difference. This reduction in electrostatic symmetry would be expected to enhance the intensity of some vibrations which could give rise to a peak (or peaks) in the difference spectra.

The remaining parameter in eq 2 is r, which, for nonadiabatic systems, is rigorously the distance separating the centroids of the donor and acceptor orbitals involved in the electron transfer. Historically, r has often been assumed to be the geometric distance separating the metal centers in symmetrical mixed-valence complexes. Recently, however, analysis of dipole moment shifts from Stark spectroscopy measurements together with other optical data have indicated that, for some systems, r is considerably shorter than the metal−metal separation.[14−16]

(36) In ref 21 we ignored the symmetry-lowering effect of the trigonal distortion and assumed the spin−orbit coupling dominated. Furthermore, we also assumed that the transition between different spin−orbit states had a simple population-weighted intensity. These erroneous assumptions probably introduced a ∼5% error in the values of H_{12} reported but do not alter the general conclusions. Additionally, we did not use parameters obtained from the reduced absorption spectrum in the calculations of H_{12} in that paper. However, as is shown here, using the parameters from the actual spectrum does not introduce any significant error in those calculations.

(37) It needs to be pointed out that eq 2 assumes the peak in the reduced absorption spectrum is Gaussian in shape, whereas, in our analysis of the titration data, we assume the actual band shape (ϵ vs ν) is Gaussian. However, multiplying the intensities of a Gaussian centered at 7470 cm^{-1} with a width of either 3200 or 4180 cm^{-1} by the corresponding frequency results in another slightly shifted Gaussian-shaped peak, so assuming that ϵ of ν is Gaussian is reasonable here. Furthermore, the value of H_{12}^{op} calculated using the parameters obtained from the reduced absorption spectrum is essentially identical to the value calculated from the parameters obtained from the ϵ vs ν spectrum. Apparently, using parameters from this latter spectrum instead of the reduced absorption spectrum to calculate H_{12}^{op} (as is frequently done) is not an unreasonable approximation.

(38) Curtis, J. C.; Meyer, T. J. *Inorg. Chem.* **1982**, *21*, 1562.

This occurs for systems that do not have high symmetry about the metal centers and/or that have strong D−A coupling.[15] For **[Fe(440)$_3$Fe]$^{5+}$**, however, neither of these situations exists. It is reasonable, therefore, to assume that, for this complex, the true value of r is very nearly the same as the metal−metal separation, d, determined from MM calculations. Moreover, application of GMH theory[16] to **[Fe(440)$_3$Fe]$^{5+}$** provides an independent theoretical estimate of r. As will be discussed below, the theoretical value of r thus obtained on the basis of CI results is, within experimental error, the same as the internuclear Fe−Fe separation resulting from the modeled structures (additional SCF results reported below suggest an upper limit of ∼10% for the likely reduction of r relative to the magnitude of d). Thus, we are confident that r in the present case is, in fact, quite close in magnitude to d, and we shall use $d = 8.9 \pm 0.2$ Å as an estimate for r in the analysis of the optical data. We note that the value of r (a property of the charge-localized diabatic states) is, in general, distinct from that for the corresponding effective electron-transfer distance inferred from the spectroscopic (adiabatic) states probed by Stark spectroscopy,[14,15] although in some cases the two effective distances are found to be quite similar (e.g., see ref 15).

There is one more structural factor that needs to be discussed. While there is every reason to believe that the structure presented in Figure 1 is the global minimum energy conformation of **[Fe(440)$_3$Fe]$^{5+}$** in solution, there are probably slightly higher energy conformers which are energetically accessible involving relatively low-frequency torsional motions about the Fe−Fe vector.

In an effort to evaluate this possibility, additional molecular modeling calculations were conducted to determine the energetic and structural consequences of torsional motion about the Fe−Fe axis, as defined by the angle ϕ introduced above. An average value for ϕ of 33° is obtained for the three bridging ligands in the low energy structure. When all three of these torsions are constrained to 23°, the energy of the structure increases by a minimum of ∼5kT (at room temperature) when no electrostatic effects are considered. When ϕ is increased to 43°, the energy increase found was only ∼1kT. As expected, in neither case does d change significantly (<0.2 Å) as long as the bridges do not "kink". Kinking a bridge in the twisted structures has roughly the same effect on energy and d as discussed in the Results section for the untwisted conformation. Since the D−A distance is unchanged with this torsional motion, there is no effect seen in the application of eq 2, but the theoretical calculations of H_{12}^{op} discussed below are found to be somewhat sensitive to these torsional motions.

To summarize the IT band spectral data obtained at 303 K, $\epsilon_{IT} = 0.24 \pm 0.01$ M^{-1} cm^{-1}, $\Delta\nu_{1/2} = 3200 \pm 200$ cm^{-1}, and $\nu_{IT} = 7470 \pm 60$ cm^{-1}. Using these values to calculate a reduced absorption spectrum yields $\epsilon'_{IT} = 0.24 \pm 0.01$ M^{-1} cm^{-1}, $\nu'_{IT} = 7710 \pm 60$ cm^{-1}, and $\Delta\nu'_{1/2} = 3000 \pm 200$ cm^{-1}. Application of eq 2 using these values and $r = 8.9 \pm 0.2$ Å yields a value of $H_{12}^{op} = 5.5 \pm 0.2$ cm^{-1}. If instead the value of $\Delta\nu_{1/2} = 4180 \pm 30$ cm^{-1} (from eq 7) is used, the calculated reduced absorption spectrum changes slightly and yields $\epsilon'_{IT} = 0.23 \pm 0.01$ cm^{-1}, $\nu'_{IT} = 7880 \pm 70$ cm^{-1}, and $\Delta\nu'_{1/2} = 4070 \pm 30$ cm^{-1}. Application of eq 2 with these values yields a value of $H_{12}^{op} = 6.3 \pm 0.2$ cm^{-1}.[38] As discussed above, it is probable that the fitting procedure has introduced an error in $\Delta\nu_{1/2}$ that is not reflected in the statistical error treatment, and thus the values of H_{12}^{op} and the reorganizational energy obtained from the different calculations disagree by more than one standard deviation obtained from the standard propagation of random error. All of the above calculations of H_{12}^{op} employ no correction for refractive index. If the Birks refractive index correction factor is used with $n = 1.342$,[30c] the two values of H_{12}^{op} (from the experimental and calculated width, respectively) become 5.4 ± 0.2 and 4.7 ± 0.2 cm^{-1} and the Chako correction factor yields 5.8 ± 0.2 and 5.0 ± 0.2 cm^{-1}, respectively.

Thermal Electron Transfer. Eq 1 relates the rate of a thermally activated electron exchange to the total reorganizational energy, λ, and the D−A coupling, H_{12}^{th}. This relation is appropriate in the high temperature classical limit for a nonadiabatic, thermoneutral electron transfer process. The weak coupling clearly places **[Fe(440)$_3$Fe]$^{5+}$** in the nonadiabatic regime. Moreover, since the activation barrier is entirely determined by low-frequency solvent modes (i.e., fully classical, vide supra) any enhancement of the rate (over that predicted by eq 1) by nuclear tunneling is highly unlikely, and can be neglected.

The most probable source of nonrandom error in the rates obtained from the NMR data is the necessity of using **[Fe(440)$_3$Ru]$^{5+}$** as the model for **[Fe(440)$_3$Fe]$^{5+}$** in the absence of electron exchange. The assumptions implicit in this model are that the magnetic environments about the Fe(II) and Ru(II) metal centers are identical and that the two complexes are isostructural.

While the magnetic environments about Fe and Ru are not exactly the same, they are likely close enough for the approximation to be valid. For example, in **[Fe(440)$_3$Ru]$^{4+}$**, the methyl peak on the iron side of the complex and the one on the ruthenium side are only 0.01 ppm offset in chemical shift. Additionally, the peak for the exchanging methyl group of **[Fe(440)$_3$Fe]$^{5+}$** comes almost exactly at the average of the corresponding peaks in the spectrum of **[Fe(440)$_3$Ru]$^{5+}$** (at every temperature the peak is shifted approximately 4% closer to the Ru^{2+} peak than predicted by this average). It is clear from these findings that substituting Ru for Fe does not significantly perturb the magnetic environment about the methyl protons.

The assumption that **[Fe(440)$_3$Ru]$^{5+}$** and **[Fe(440)$_3$Fe]$^{5+}$** are isostructural is also fairly benign. While there is a 0.1 Å M−N bond length increase upon replacing Fe with Ru in $[M(bpy)_3]^{2+}$,[31a,39] the effect on d in **[Fe(440)$_3$M]$^{5+}$** is negligible. The difference in M−N bond lengths between the two complexes occurs along a direction perpendicular to the M−M axis of the molecule; thus, the Fe−M distance is basically the same in **[Fe(440)$_3$Fe]$^{5+}$** and **[Fe(440)$_3$Ru]$^{5+}$**.

The other potential sources of error, intermolecular electron exchange and intermolecular paramagnetic effects, were ruled out from concentration studies. In some of the higher concentration samples at higher temperature, NMR spectra exhibited broadening of the diamagnetic peaks due to intermolecular effects, and those spectra were omitted from the rate calculations.

The rate constants for the electron self-exchange in **[Fe(440)$_3$Fe]$^{5+}$** are listed in column 2 of Table 2. These values can be used to extract H_{12}^{th} from the Arrhenius-type plot presented in Figure 6. To get a connection between the electron-transfer parameters and the Arrhenius coefficients A and B in eq 8 we have assumed that the total classical reorganizational

$$\ln(k_{ET}\sqrt{T}) = A + B\left(\frac{1}{T}\right) \tag{8}$$

energy in eq 1 is composed of a temperature-independent intramolecular part (which is effectively zero in the present case) and the solvent reorganizational energy, $\lambda(T)$. Then, from eqs 1 and 8, noting that the temperature dependence of λ in the

(39) Rillema, D. P.; Jones, D. S.; Woods, C.; Levy, H. A. *Inorg. Chem.* **1992**, *31*, 2935.

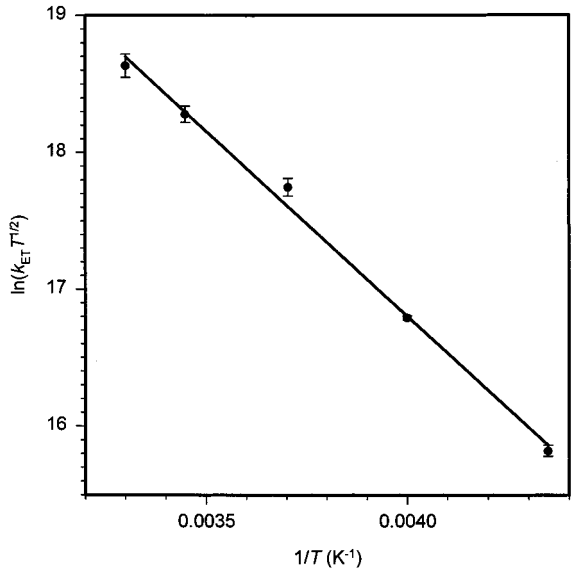

Figure 6. Arrhenius-type plot of temperature-dependent electron exchange rate constants for **[Fe(440)$_3$Fe]$^{5+}$**. The circles correspond to k_{ET} obtained from analysis of the methyl peak. The solid line is the best fit of the data using eqs 8−10 with $(\partial\lambda/\partial T)_P = 0$.

pre-exponent is negligible, we have

$$A = \ln\left(\frac{2(H_{12}{}^{th})^2}{h}\sqrt{\frac{\pi^3}{\lambda(T_0)k}}\right) - \frac{1}{4k}\left(\frac{\partial\lambda}{\partial T}\right)_P \qquad (9)$$

and

$$B = -\frac{\lambda(T_0)}{4k} - \frac{T_0}{4k}\left(\frac{\partial\lambda}{\partial T}\right)_P \qquad (10)$$

In eqs 9 and 10, T_0 is the temperature in the experimental temperature range at which $(\partial\lambda/\partial T)_P$ is evaluated (298 K). If we assume $(\partial\lambda/\partial T)_P = 0$, the Arrhenius fit yields $H_{12}{}^{th} = 15 \pm 3$ cm^{-1} and $\lambda = 7500 \pm 300$ cm^{-1}. To understand the effect of temperature variations in λ on calculated values of $H_{12}{}^{th}$ one can start with the classical Marcus equation for outer-sphere reorganization[30a]

$$\lambda = e^2 c_0(1/a - 1/d) \qquad (11)$$

where $c_0 = 1/\epsilon_\infty - 1/\epsilon_s$ is the Pekar factor and we assume the donor−acceptor complex to be composed of two spheres of radius a with $d = 8.9$ Å. Now, if we use temperature-dependent high-frequency, ϵ_∞, and static, ϵ_s,[40d] dielectric constants for acetonitrile in eq 11 and fit eq 11 to the experimental value of the reorganizational energy obtained optically, $\lambda = 7900$ cm^{-1} to get a, we arrive at $(\partial\lambda/\partial T)_P = 5.5$ cm^{-1} K^{-1}. When used in eq 8, this temperature derivative yields $H_{12}{}^{th} = 40 \pm 7$ cm^{-1}. The magnitude and the sign of $(\partial\lambda/\partial T)_P$ are thus important parameters substantially affecting the value of $H_{12}{}^{th}$ extracted from the Arrhenius intercept: $H_{12}{}^{th}$ increases for $(\partial\lambda/\partial T)_P > 0$ and decreases for $(\partial\lambda/\partial T)_P < 0$. To obtain a more accurate estimate of the temperature derivative of the reorganizational energy we employed here a molecular description of solvent reorganization developed by one of us.[40]

(40) (a) Matyushov, D. V. *Mol. Phys.* **1993**, *79*, 795. (b) Matyushov, D. V. *Chem. Phys.* **1993**, *174*, 199. (c) Matyushov, D. V.; Schmid, R. *J. Phys. Chem.* **1994**, *98*, 5152. (d) Matyushov, D. V.; Schmid, R. *Chem. Phys. Lett.* **1994**, *220*, 359.

Solvent reorganization in molecular liquids is composed of two major parts, the energy invested in reorienting the solvent dipoles, λ_{or}, and the energy of reorganizing the solvent density near the donor−acceptor complex, λ_d.[40]

$$\lambda = \lambda_{or} + \lambda_d \qquad (12)$$

The orientational component λ_{or} changes with temperature essentially as predicted by continuum theories; i.e., for sufficiently polar solvents $(\partial\lambda_{or}/\partial T)_P > 0$. On the contrary, the density component, λ_d, contains an explicit $\propto T^{-1}$ temperature dependence and thus decreases with temperature. For polar solvents such as acetonitrile the decrease in λ_d usually overrides the increase in λ_{or}, and the total solvent reorganizational energy, λ, tends to decrease with increasing T.

The temperature-dependent reorganizational energy was calculated according to the molecular theory developed in ref 40b. First, representing the donor and acceptor units by spheres of radius a at a distance d, we obtain a by fitting the experimental optical reorganizational energy, $\lambda = 7900$ cm^{-1} (obtained from the reduced absorption spectrum), to that calculated in the molecular theory[40] at $T_0 = 298$ K. This gives $a = 4.44$ Å. Then the temperature-dependent λ_{or} was calculated in the experimental temperature range 230−303 K. The derivative $(\partial\lambda_{or}/\partial T)_P = 4.7$ cm^{-1} K^{-1} is, as mentioned above, close to the magnitude predicted from the continuum theory. The reason is the common mechanism of orientational fluctuations implied in both treatments. In contrast, the temperature derivative of the density component is negative, $(\partial\lambda_d/\partial T)_P = -11.3$ cm^{-1} K^{-1}, resulting in the negative temperature derivative of the total solvent reorganizational energy $(\partial\lambda/\partial T)_P = -6.6$ cm^{-1} K^{-1}. When the latter estimate is used in eq 8, we arrive at $H_{12}{}^{th} = 4.7 \pm 0.9$ cm^{-1}.

Analogous to the situation discussed above for $H_{12}{}^{op}$, $H_{12}{}^{th}$ may also be viewed as an effective (rms) matrix element reflecting the underlying roles of the A → A and E' → E' components, as controlled by the spin−orbit (λ_{so}) and spatial splitting (Δ) parameters. In contrast to the optical case (see eq 6 and subsequent discussion), which is the rms result based on equal-weighted contributions from the $\Psi_1 \rightarrow \Psi_1$ and $\Psi_1 \rightarrow \Psi_2$ transitions (where the initial and final states are charge-localized at the two respective Fe^{3+} sites), the weighting is estimated to be somewhat different in the thermal case (e.g., ∼70% and 30%, respectively for the limiting case of zero torsional angles (ϕ)). Such estimates may be obtained using an approach of the type employed previously for the analogous case of electron exchange between spin−orbit mixed states of $Co(NH_3)_6{}^{2+/3+}$ (see eqs 27 and 30 and related discussion in ref 20c). Thus, some difference in $H_{12}{}^{op}$ and $H_{12}{}^{th}$ magnitudes is possible. Nevertheless, the analysis of the optical and thermal data is found (below) to yield very similar values for $H_{12}{}^{op}$ and $H_{12}{}^{th}$.

Comparison of Optical and Thermal Results. Our goal in this study has been to quantitatively compare the theories of thermal and optical electron-transfer embodied in eqs 1 and 2, respectively. The two parameters on which this comparison rests are the donor−acceptor coupling matrix element, H_{12}, and the reorganizational energy, which corresponds to λ in eq 1 and the maximum of the reduced absorption spectrum, ν'_{IT}, in the Hush treatment. Table 3 contains the values of H_{12} and the reorganizational energy obtained from the two treatments with various corrections in place. The reorganizational energy is obtained directly from the reduced absorption spectrum, and $H_{12}{}^{op}$ is calculated from eq 2 in the Hush treatment. All of the uncertainties in the values used in the calculation of $H_{12}{}^{op}$ were statistically determined. Standard propagation of error tech-

Table 3. Experimentally Determined Values of H_{12}^{op}, H_{12}^{th}, and Reorganizational Energies for **[Fe(440)$_3$Fe]$^{5+}$**

Optical			
refractive index correction	$f(n)$ ($n = 1.342$)[a]	H_{12}^{op} (cm^{-1})[b]	reorganizational energy (cm^{-1})[c]
Birks	n^3	5.4 ± 0.7	
Chako	$n(n^2+2)^2/9$	5.8 ± 0.7	7900 ± 200
none	$(n^2/(f(n)=1)$	6.3 ± 0.8	
Thermal			
temperature correction model	$(\partial\lambda/\partial T)_P$ (cm^{-1} K^{-1})	H_{12}^{th} (cm^{-1})[d]	reorganizational energy (cm^{-1})[d]
none	0	15 ± 3	
continuum[e]	5.5	40 ± 7	7500 ± 300
molecular[f]	-6.6	4.7 ± 0.9	

[a] Found in ref 30c. [b] Calculated using eq 2. [c] Obtained from the calculated reduced absorption spectrum of the IT band. [d] Obtained from best fits of eqs 8−10 to plots of $\ln(k_{ET}T^{1/2})$ vs T^{-1}. [e] The two-spheres in a dielectric continuum model in ref 30a. [f] The treatment developed in ref 40 (see text).

niques were then used to find the error in H_{12}^{op} in both calculations: the one using the experimental $\Delta\nu_{1/2}$ and the one using the theoretical width. It is clear from comparing the results from these two calculations that both H_{12}^{op} and its uncertainty are relatively insensitive to which width is used. However, in the interest of conservatism, it may be prudent to increase the uncertainty in H_{12}^{op} to equal the difference between the two calculated values. Assuming the width predicted by eq 7 to be the more accurate value, one obtains a spectrally determined coupling matrix element $H_{12}^{op} = 6.3 \pm 0.8$ cm^{-1} if no refractive index correction is included. For the Birks and Chako refractive index corrections, H_{12}^{op} values with the extended error bars are 5.4 ± 0.7 cm^{-1} and 5.8 ± 0.7 cm^{-1}, respectively. A similar increase in the error bars for the reorganizational energy obtained from the maximum of the reduced absorption spectrum, ν'_{IT}, is also reasonable. If the value obtained assuming the calculated width is again believed to be more accurate, a reorganizational energy of 7900 ± 200 cm^{-1} results.

Fit of eqs 8−10 to the rate constant data in Table 2 with $(\partial\lambda/\partial T)_P = 0$ results in a value for H_{12}^{th} (15 ± 3 cm^{-1}) that differs from H_{12}^{op} (6.3 ± 0.8, 5.4 ± 0.7, and 5.8 ± 0.7 cm^{-1} using no correction, the Birks correction, and the Chako correction, respectively) at better than the 95% confidence level. The value of λ resulting from the same fit is, however, in good agreement with the value for the reorganizational energy obtained from the optical measurement (7900 ± 200 obtained from the calculated reduced absorption spectrum vs 7500 ± 300 cm^{-1} extracted from the Arrhenius-type plot assuming $(\partial\lambda/\partial T)_P = 0$). The main source of the difference in H_{12} values is associated with the evaluation of the temperature dependence of the reorganizational energy. If classical dielectric continuum theory is applied to predict $(\partial\lambda/\partial T)_P$, a value for H_{12}^{th} of 40 ± 9 cm^{-1} results, worsening the agreement between H_{12}^{op} and H_{12}^{th}. However, if a molecular level model is employed to determine $(\partial\lambda/\partial T)_P$, H_{12}^{th} becomes 4.7 ± 0.9 cm^{-1}, in much better agreement with H_{12}^{op}.

Theoretical Estimates and Analysis of H_{12}^{op} and r. Estimates of H_{12}^{op} and r were obtained by analyzing the calculated results for the relevant spectroscopic states in terms of the generalized Mulliken−Hush model, implemented at the "two-state" level. The two-state space is that dominated by the two *A*-symmetry (see above) hole states largely localized on the two Fe sites (as noted above, analogous calculations for coupling within the *E*-symmetry manifold yielded similar magnitudes). The eigenstates of the *A*-symmetry space were obtained from CI calculations based on two charge-localized CI basis configurations. These latter were constructed from a common orthonormal set of MOs (molecular orbitals) obtained from 2-state-averaged SCF (2-SA/SCF) calculations of the same type as described in the earlier study.[21]

Table 4. H_{12}^{op} Values for **[Fe(4x0)$_3$Fe]$^{5+}$**

	$\lvert H_{12}^{op}\rvert$ (cm^{-1})	
[Fe(L)$_3$Fe]$^{5+}$, L	experimental[a]	calculated[b]
full complex		
420	19 ± 3	60 (46[c,d])
430	57 ± 9	46 (52[c,e])
440	6.3 ± 0.8	0.23 ($\phi = 33°$)[f]
		0.37 ($\phi = 23°$)[f]
		0.70 ($\phi = 43°$)[f]
tethers removed[g]		
420		104 (97[c,d])
430		46 (52[c,e])
440		3.2 ($\phi = 33°$)[f]
		6.8 ($\phi = 23°$)[f]
		1.3 ($\phi = 43°$)[f]

[a] Values were calculated with no correction for refractive index. [b] Except as noted otherwise, calculated results are based on the minimum energy MM structure obtained in the present work. [c] From ref 21. [d] Based on coordinates taken from the reported crystal structure.[41] [e] Based on the MM structure reported in ref 21. [f] Based on three conformational variants defined by the dihedral angle, ϕ (see text): the equilibrium structure ($\phi = 33°$) and structures obtained subject to the constraint of a twist of $\pm 10°$. [g] Based on truncated structures obtained by removal of tethers and patching of disrupted bonds with hydrogen atoms, all other coordinates being left fixed.

The GMH model yields eqs 13 and 14

$$r = (|\Delta\vec{\mu}_{12}|^2 + 4|\vec{\mu}_{12}|^2)^{1/2}/e \tag{13}$$

$$|H_{12}| = \frac{|\vec{\mu}_{12}|}{er}\Delta E_{12} \tag{14}$$

where $\Delta\mu_{12}$ is the dipole moment difference between the two spectroscopic states (eigenvectors), μ_{12} is the component of the corresponding transition dipole moment along the $\Delta\mu_{12}$ vector, e is the magnitude of the electronic charge, and ΔE_{12} is the spectroscopic transition energy.[16] For simplicity, we present the expression for the *magnitude* of H_{12}. The sign of H_{12} may also be determined once a phase convention for the various orbitals and states has been defined. The values of H_{12}^{op} obtained from calculations done on **[Fe(440)$_3$Fe]$^{5+}$**, along with some other relevant data, are presented in Table 4.

As in the case of the **[Fe(420)$_3$Fe]$^{5+}$** and the **[Fe(430)$_3$Fe]$^{5+}$** systems dealt with earlier,[21] the r value calculated for **[Fe(440)$_3$Fe]$^{5+}$** at the 2-SA/SCF level is within 0.01 Å of d, thus supporting the use of this latter value in the implementation of eq 2 reported above.[42] Additional calculations of the single-configuration SCF type were carried out to provide bounds for the likely departure of r from d.[43] These results, together with the CI results given above, suggest upper and lower bounds for r of d and $\sim 0.9d$, respectively.

(41) Serr, B. R.; Andersen, K. A.; Elliott, C. M.; Anderson, O. P. *Inorg. Chem.* **1988**, *27*, 4499.

(42) Calculations were also carried out with an extended CI basis (defined in terms of the 2A-SA/SCF orbitals) which included all single excitations from a doubly filled MO to an "active MO" (one of the two dominated by d_{z^2} AOs at the respective Fe sites) and also all single excitations from an active MO to an empty one. These extended CI calculations yielded only $\sim 1-2\%$ changes in r values and uniformly increased H_{12} magnitudes by a factor of ~ 2.

In addressing the nature of the coupling which leads to the observed trend in experimental H_{12}^{op} values for **[Fe(420)$_3$Fe]$^{5+}$**,[21,36] **[Fe(430)$_3$Fe]$^{5+}$**,[21,36] and **[Fe(440)$_3$Fe]$^{5+}$** (i.e., 19, 57, and 6.3 cm^{-1}), we note that relative to the **[Fe(430)$_3$Fe]$^{5+}$** value, the **[Fe(420)$_3$Fe]$^{5+}$** and **[Fe(440)$_3$Fe]$^{5+}$** values may at first glance be considered surprisingly small: i.e., one might expect the **[Fe(420)$_3$Fe]$^{5+}$** value to be at least as great as the **[Fe(430)$_3$Fe]$^{5+}$** value, given the shorter tether for **[Fe(420)$_3$Fe]$^{5+}$**, and the very similar r values for the two systems;[21,45] likewise the reduction by a factor of ~10 in proceeding from **[Fe(430)$_3$Fe]$^{5+}$** to **[Fe(440)$_3$Fe]$^{5+}$** corresponds to an increase of only one additional C−C bond in each tether and an increase of only ~1.3 Å in the Fe−Fe separation. The situation regarding **[Fe(420)$_3$Fe]$^{5+}$** vs **[Fe(430)$_3$Fe]$^{5+}$** was rationalized previously by recognizing that the net **[Fe(420)$_3$Fe]$^{5+}$** coupling arises from significant destructive interference between "through bond" (TB) coupling (via the tethers) and "through space" (TS) coupling (directly between the members of an adjacent pair of bpy groups), whereas the **[Fe(430)$_3$Fe]$^{5+}$** coupling arises almost exclusively from the TS pathways.[21]

These results may be understood in the context of the "parity" rule,[46] which for fully staggered alkyl spacers with an *odd* number of spacer CC bonds (as in the case of **[Fe(420)$_3$Fe]$^{5+}$**) predicts *destructive* TB and TS interference, while for *even* numbers of spacer bonds, *constructive* interference is expected.[47] When the tethers are not fully staggered (as for the present tethered systems) the quantitative situation is more complex. For the **[Fe(420)$_3$Fe]$^{5+}$** system (where the tether has a gauche conformation) the predictions of the simple parity rule are qualitatively observed, and model calculations have demonstrated the occurrence of appreciable destructive interference.[21] The highly constricted geometry of some of the torsion angles in the **[Fe(430)$_3$Fe]$^{5+}$** tethers (between cis and gauche conformations) effectively suppresses all TB contributions. Since the **[Fe(440)$_3$Fe]$^{5+}$** tethers have odd numbers of CC bonds and torsional angles either staggered (about central CC bonds) or gauche (about peripheral CC bonds), one expects (as for **[Fe(420)$_3$Fe]$^{5+}$**) significant destructive interference, consistent with the observed **[Fe(440)$_3$Fe]$^{5+}$** H_{12}^{op} value relative to that for **[Fe(430)$_3$Fe]$^{5+}$**.

The calculated H_{12}^{op} values based on the GMH analysis of the CI results (eqs 13 and 14) are in qualitative conformity with the above expectations, although the calculations are not able to give a quantitatively reliable account of the competition between TS and TB contributions. Thus, the calculated results for **[Fe(420)$_3$Fe]$^{5+}$** and **[Fe(430)$_3$Fe]$^{5+}$** are quite similar in magnitude (respectively, 46 and 52 cm^{-1})[48] in contrast to the significant difference between the corresponding experimental estimates (H_{12}^{op} = 19 and 57 cm^{-1}, respectively). Furthermore, the calculated results for **[Fe(440)$_3$Fe]$^{5+}$** (≲1 cm^{-1}) imply an exaggerated degree of TS/TB cancellation.[49] While this may in part reflect defects inherent in the INDO/S parametrization, which emphasizes bonded interactions, we note that INDO/S treatment of a number of other long-range electron-transfer processes (spanning donor−acceptor separations from 6 to 11 Å)[50] has not revealed major systematic errors.

Since variations in the energy of the **[Fe(440)$_3$Fe]$^{5+}$** system with respect to the relative torsional angle of the Fe(bpy)$_3$ moieties correspond to fairly low energy fluctuations (the MM model yields a force constant of ~0.9mdyne·Å/rad^2), it is of interest to estimate the sensitivity of calculated H_{12}^{op} magnitudes to this degree of freedom. The calculations yield variation of H_{12}^{op} magnitudes by a factor of ~3 over a range of angles within ±10° of calculated equilibrium torsional angle (see Table 4). The same degree of variation is also displayed by the H_{12}^{op} values for the system with the tethers removed (see Table 4).

Conclusion

The mixed-valence complex **[Fe(440)$_3$Fe]$^{5+}$** is a rare chemical system for which it is possible to obtain both rates of thermal electron transfer and parameters for the optical intervalence charge-transfer transition. Obtaining both types of data from a single chemical system has provided a platform for comparison between the two classical theories which describe these different but intimately related phenomena. Moreover, the reorganizational energy for the electron transfer in **[Fe(440)$_3$Fe]$^{5+}$** is governed exclusively by low frequency solvent modes, providing an unprecedented opportunity to compare the parameters predicted by each theory at the classical level, free from the usual complications and ambiguities.

The two parameters common to both theories are the reorganizational energy and the donor−acceptor coupling matrix element, H_{12}. To the extent that no systematic errors have been introduced into any of the experimental results or associated assumptions, eqs 1 and 2 yield reorganizational energies in good agreement (7900 ± 200 and 7500 ± 300 cm^{-1}, respectively) for intramolecular electron transfer in **[Fe(440)$_3$Fe]$^{5+}$**. The donor−acceptor coupling matrix element extracted from the intercept of the Arrhenius plot is dramatically affected by the assumptions made about the temperature dependence of the solvent reorganizational energy.[28] For the temperature derivative of the reorganizational energy calculated from the continuum Marcus expression, from the temperature independence assumption, and from the molecular treatment,[40] the values of H_{12}^{th} are 40 ± 7, 15 ± 3, and 4.7 ± 0.9 cm^{-1}, respectively. The latter value agrees best with the experimental optical results, 6.3 ± 0.8, 5.4 ± 0.7, or 5.8 ± 0.6 cm^{-1}, depending on the refractive index correction employed. This analysis indicates that caution should be used in applying the continuum model when treating phenomena for which temperature variation of the reorganizational energy is important.

(43) The use of state-averaged SCF calculations (such as the present 2-SA/SCF) tends to suppress some of the state-specific polarization associated with charge-localized states (i.e., the polarization of the reduced site (2+) by the oxidized site (3+)),[9] an effect which can lead to a reduction in the net r value, as pointed out by Reimers and Hush.[44] Accordingly, we also evaluated r on the basis of single-configuration SCF charge-localized states, obtaining for **[Fe(440)$_3$Fe]$^{5+}$** a value of $r = 0.9d$. Although these results are not directly amenable to GMH analysis (since the two SCF states are not orthogonal), they nevertheless serve to provide an upper limit for the reduction of r relative to d.

(44) Reimers, J. R.; Hush, N. S. *J. Phys. Chem.* **1991**, *95*, 9773.

(45) The Fe−Fe distances, d, for **[Fe(420)$_3$Fe]$^{5+}$** and **[Fe(430)$_3$Fe]$^{5+}$** are practically identical at ~7.6 Å.

(46) (a) Paddon-Row, M. N. *Acc. Chem. Res.* **1982**, *15*, 245. (b) Verhoeven, J. W.; Pasman, P. *Tetrahedron* **1981**, *37*, 943.

(47) This expectation is based on the fact that the TS coupling of the pyridine pairs is bonding, while the corresponding TB coupling via the tethers is generally antibonding (bonding) for an odd (even) number of tether bonds. See refs 9 and 21.

(48) These values, based, respectively, on X-ray data and a MM model, were reported in ref 21. Subsequent calculations based on refined MM minimization yield values of 60 and 46 cm^{-1}.

(49) The TS contribution to H_{12} is estimated to be ~3 cm^{-1}, based on the calculated result for the equilibrium structure of the [Fe(440)$_3$Fe]$^{5+}$ system but with the tethers removed (keeping all other atomic coordinates fixed and capping the disrupted bonds with hydrogen atoms). The closest carbon−carbon separation distance between adjacent pyridyl groups is 4.8 Å, considerably shorter than the Fe−Fe separation, d = 8.9 ± 0.2 Å.

(50) (a) Newton, M. D.; Ohta, K.; Zhong, E. *J. Phys. Chem.* **1991**, *95*, 2317. (b) Cave, R. J.; Newton, M. D.; Kumer, K.; Zimmt, M. B. *J. Phys. Chem.* **1995**, *99*, 17501. (c) Sachs, S. B.; Dudek, S. P.; Hsung, R. P.; Sita, L. R.; Smalley, J. F., Newton, M. D.; Feldberg, S. W.; Chidsey, C. E. D. *J. Am. Chem. Soc.* **1997**, *119*, 10563.

Analysis of the calculated CI results in terms of the GMH model reveals a high degree of destructive interference between tunneling pathways involving the **440** tethers and TS pathways involving direct coupling between adjacent bpy moieties, similar to the result also found for the other tethers with an even number of C−C bonds (**420**) but not for those with an odd number of bonds (**430**). This qualitative behavior is in conformity with simple superexchange concepts, although the quantitative details are dependent on the conformation of the tethers. The degree of destructive interference yielded by the present calculations for the **[Fe(440)$_3$Fe]**$^{5+}$ system is found to be exaggerated with the resulting H_{12}^{op} estimate ($\lesssim$1 cm^{-1}) appreciably smaller than the experimental estimate (6.3 $\pm$ 0.8, 5.4 $\pm$ 0.7, or 5.8 $\pm$ 0.7 cm^{-1}).

Finally, the CI-based GMH estimates of r are found in all cases to be within 2% of the corresponding Fe−Fe separation distances, d, thus reflecting the high degree of local symmetry at the Fe sites, in contrast to other situations in which less symmetric metal−ligand coordination shells may yield r values considerably smaller than d values. A lower limit of $r \cong 0.9d$ is inferred from single-configuration charge-localized SCF calculations.

Acknowledgment. The authors acknowledge support of this work from the Division of Chemical Sciences, Office of Basic Energy Science, U.S. Department of Energy, under Grants DE-FG03-97ER14808 (C.M.E.) at Colorado State University and DE-AC02-98CH10886 (M.D.N.) at Brookhaven National Laboratory. Support from the National Science Foundation, Grant CHE-9520619 (D.V.M.), is also acknowledged. Finally, we acknowledge a number of valuable comments made by the reviewers.

JA981067D